J. Fluid Mech. (2014), *vol.* 745, *pp.* 487–508.
doi:10.1017/jfm.2014.66

Effects of membrane hardness and scaling analysis for capsules in planar extensional flows

P. Dimitrakopoulos†

Department of Chemical and Biomolecular Engineering, University of Maryland, College Park, MD 20742, USA

(Received 8 May 2013; revised 30 December 2013; accepted 24 January 2014; first published online 24 March 2014)

In this paper, we investigate computationally the effects of membrane hardness on the dynamics of strain-hardening capsules in planar extensional Stokes flows. As the flow rate increases, all capsules reach elongated steady-state configurations but the cross-section of the more strain-hardening capsules preserves its elliptical shape while the less strain-hardening capsules become lamellar. The capsule deformation in strong extensional flows is accompanied with very pointed edges, i.e. large edge curvatures and thus small local edge length scales, which makes the current investigation a multi-length interfacial dynamics problem. Our computational results for elongated strain-hardening capsules are accompanied with a scaling analysis which provides physical insight on the extensional capsule dynamics. The two distinct capsule conformations we found, i.e. the slender spindle and lamellar capsules, are shown to represent two different types of steady-state extensional dynamics. The former are stabilized mainly via the membrane's shearing resistance and the latter via its area-dilatation resistance, associated with the elongation tension normal forces and thus both types differ from bubbles which are stabilized mainly via the lateral surface-tension normal forces. Our steady-state deformation results can be used to identify the elastic properties of a real capsule, i.e. the membrane's shear and area-dilatation moduli, utilizing a single experimental technique.

Key words: biological fluid dynamics, boundary integral methods, membranes

1. Introduction

The study of the interfacial dynamics of artificial or physiological capsules (i.e. membrane-enclosed fluid volumes) in Stokes flow has seen an increased interest during the last few decades due to their numerous engineering and biomedical applications. Artificial capsules have wide applications in the pharmaceutical, food and cosmetic industries (Pozrikidis 2003). In pharmaceutical processes, for example, capsules are commonly used for the transport of medical agents. Additional applications include cell sorting and cell characterization devices (Cranston *et al.* 1984; Alexeev & Balazs 2007; Fiddes *et al.* 2007; Chabert & Viovy 2008) and fabrication of microcapsules with desirable properties (Lensen *et al.* 2010; Seiffert *et al.* 2010). The motion of red blood cells through vascular microvessels has long

† Email address for correspondence: dimitrak@umd.edu

been recognized as a fundamental problem in physiology and biomechanics, since the main function of these cells, to exchange oxygen and carbon dioxide with the tissues, occurs in capillaries (Popel & Johnson 2005).

The determination of the mechanical properties for the membrane of artificial or physiological capsules is essential for the better design of the various devices in which they are utilized (Leclerc *et al.* 2012; Koleva & Rehage 2012). For this, several techniques have been developed including static compression and shear or centrifugal flow fields for millicapsules as well as micropipette and atomic force microscope measurements, and flow in microfluidic channels and tubes for microcapsules (see e.g. Pieper, Rehage & Barthès-Biesel 1998; Carin *et al.* 2003; Prevot *et al.* 2003; Dimitrakopoulos 2012; Koleva & Rehage 2012; Leclerc *et al.* 2012). We emphasize that the membrane mechanical determination of a capsule is still a challenging task, especially for the characterization of both the membrane's shear and area-dilatation moduli, where two experimental techniques are commonly required (Pieper *et al.* 1998; Koleva & Rehage 2012).

The aforementioned applications have motivated the study of artificial capsules in linear flows, such as simple shear and planar extensional flows, which reveal the fundamental capsule physics in extensional and rotational flow dynamics. Experimental studies on capsule deformation have investigated both simple shear and extensional flows (e.g. Barthès-Biesel 1991; Chang & Olbricht 1993*a*,*b*; Koleva & Rehage 2012). Computational investigations have also considered capsules in weak, moderate and strong linear flows, especially in recent years facilitated by the development of more powerful and diverse numerical methodologies (e.g. Lac *et al.* 2004; Dodson & Dimitrakopoulos 2008; Kessler, Finken & Seifert 2008; Dodson & Dimitrakopoulos 2009; Walter *et al.* 2010; Kumar & Graham 2012).

In the area of interest of the present study (i.e. capsule dynamics in planar extensional flows), the asymptotic solutions for initially spherical capsules by Barthès-Biesel and coworkers are restricted to small deformations (see e.g. Barthès-Biesel & Rallison 1981; Barthès-Biesel 1991; Barthès-Biesel, Diaz & Dhenin 2002). Experimental studies on capsule deformation in extensional flows are still very limited in number and restricted to small and moderate deformations (Barthès-Biesel 1991; Chang & Olbricht 1993*a*), even though the required flow rates for large capsule deformations have long been achieved in corresponding experiments with droplets and bubbles in four-roll mill devices (Bentley & Leal 1986; Ha & Leal 2001). Chang & Olbricht (1993*a*) investigated synthetic capsules (made from a thin nylon membrane) in small and moderate deformations only owing to experimental limitations, where the capsules obtain steady-state elliptical profiles. This is also the range studied in the computational work of Lac *et al.* (2004) owing to computational failure at higher flow rates. In our previous paper, we investigated the dynamics of strain-hardening Skalak and strain-softening neo-Hookean capsules in strong planar extensional flows, where both capsules reach elongated steady-state configurations but the cross-section of the Skalak capsule preserves its elliptical shape while the neo-Hookean capsule becomes lamellar (Dodson & Dimitrakopoulos 2009).

More involved capsule conformations were found in extensional flow experiments with capsules made of a polylysine membrane, including stable steady-state shapes whose edges become rounded, then more extended and pointed (i.e. spindled), and finally cusped as the flow rate increases (Barthès-Biesel 1991). In our earlier letter (Dodson & Dimitrakopoulos 2008), we studied computationally the dynamics of a strain-hardening Skalak capsule in a planar extensional flow and showed that in strong flow rates, the elongated capsule develops steady-state shapes whose edges

from spindled become cusped with increasing flow rate owing to a transition of the edge tensions from tensile to compressive.

In the present study, we consider the effects of the membrane hardness on the dynamics of strain-hardening Skalak capsules in planar extensional Stokes flows. (The strain-hardening nature of these capsules enables them to withstand strong flow rates.) In particular, we investigate the steady-state properties of these capsules with increasing membrane hardness (or strain-hardening nature). The capsule deformation in strong extensional flows is accompanied with very pointed edges, i.e. large edge curvatures and thus small local edge length scales, which makes the current investigation a multi-length interfacial dynamics problem. Our computational results for elongated strain-hardening capsules are accompanied with a scaling analysis which provides useful physical insight on the capsule dynamics, revealing two different types of steady-state extensional membrane dynamics. Our steady-state deformation results can also be used to identify the elastic properties of a real capsule, i.e. the membrane's shear and area-dilatation moduli, utilizing a single experimental technique.

2. Problem description

We consider a three-dimensional spherical capsule with an elastic interface in an infinite ambient fluid. The interior and exterior fluids are Newtonian, with viscosities $\lambda\mu$ and μ, and the same density. The capsule size is specified by the radius a of its quiescent spherical shape of volume $V = 4\pi a^3/3$. Far away, the flow approaches a planar extensional flow $\boldsymbol{u}^\infty = G(x, -y, 0)$, where G is the shear rate. We assume that the Reynolds number is small for both the surrounding and the inner flows, and thus the capsule deformation occurs in the Stokes regime.

Based on the standard boundary integral formulation for interfacial dynamics in Stokes flows, the velocity $\boldsymbol{u}$ at a point $\boldsymbol{x}_0$ on the interface S_B of a freely suspended capsule may be determined by the following boundary integral equation

$$(1+\lambda)\boldsymbol{u}(\boldsymbol{x}_0) - 2\boldsymbol{u}^\infty(\boldsymbol{x}_0) = -\frac{1}{4\pi\mu}\int_{S_B} [\boldsymbol{S}\cdot\Delta\boldsymbol{f} - (1-\lambda)\mu\boldsymbol{T}\cdot\boldsymbol{u}\cdot\boldsymbol{n}](\boldsymbol{x})\,\mathrm{d}S, \qquad (2.1)$$

where $\boldsymbol{n}$ is the interfacial unit normal pointing into the surrounding fluid, and the tensors $\boldsymbol{S}$ and $\boldsymbol{T}$ are the fundamental solutions for the velocity and stress for the three-dimensional Stokes equations, respectively (Pozrikidis 2001; Lac *et al.* 2004; Dodson & Dimitrakopoulos 2009). Owing to the no-slip condition at the interface, the time evolution of the material points $\boldsymbol{x}$ of the membrane may be determined via the kinematic condition at the interface

$$\frac{\partial\boldsymbol{x}}{\partial t} = \boldsymbol{u}. \qquad (2.2)$$

To produce a closed system of equations, the surface stress $\Delta\boldsymbol{f}$ on the capsule interface is determined by the membrane dynamics. In this work, we consider elastic membranes with shearing and area-dilatation resistance but negligible bending resistance. Our membrane description is based on the well-established continuum approach and the theory of thin shells which consider the membrane as a two-dimensional continuum with in-plane isotropy (Pozrikidis 2003; Lac *et al.* 2004), as described in detail in § 2.2 of our earlier publication (Dodson & Dimitrakopoulos 2009). We emphasize that the study of capsules or cells via the continuum approach and the theory of thin shells is now a rather classical problem. Thus, here we present

a laconic description of the membrane statics; more details may be found in relevant review articles and books (see e.g. Pozrikidis 2001, 2003).

The membrane thickness for a wide range of artificial capsules and the erythrocytes is several orders of magnitude smaller than the size of the capsule/cell, and thus the thin-shell theory has proven to be an excellent description of these membranes, up to a membrane thickness of 5 % the capsule size (Pieper *et al.* 1998; Carin *et al.* 2003; Rachik *et al.* 2006; Dodson & Dimitrakopoulos 2010). In addition, we restrict our interest to elastic membranes with shearing and area-dilatation resistance but negligible bending resistance. This class represents a wide range of artificial capsules whose bending resistance is very small compared with their shearing resistance. Experimental findings for nylon capsules (Chang & Olbricht 1993*a*), aminomethacrylate capsules (Pieper *et al.* 1998) and biocompatible alginate capsules (Rachik *et al.* 2006) compare very well with theoretical models that ignore bending resistance. The cusped shape of polylysine capsules at high extensional flow rates (Barthès-Biesel 1991) reveals that the capsule membrane has negligible bending resistance. To a great extent, this model also applies to the human red blood cells where the interior haemoglobin solution is enclosed by a multilayer membrane whose reduced bending modulus (with respect to its shearing resistance) is $O(10^{-3})$ (Mohandas & Chasis 1993).

For a membrane with shearing and area-dilatation resistance considered in this work, the surface stress is determined by the in-plane stresses, i.e. $\Delta \boldsymbol{f} = -\nabla_s \cdot \tau$ which in contravariant form gives

$$\Delta \boldsymbol{f} = -\left(\tau^{\alpha\beta}|_\alpha \, \boldsymbol{t}_\beta + b_{\alpha\beta} \, \tau^{\alpha\beta} \, \boldsymbol{n}\right), \tag{2.3}$$

where the Greek indices range over 1 and 2, while Einstein notation is employed for (every two) repeated indices. In this equation, the $\tau^{\alpha\beta}|_\alpha$ notation denotes covariant differentiation, $\boldsymbol{t}_\beta = \partial \boldsymbol{x}/\partial\theta^\beta$ are the tangent vectors on the capsule surface described with arbitrary curvilinear coordinates θ^β, and $b_{\alpha\beta}$ is the surface curvature tensor (Pozrikidis 2003; Lac *et al.* 2004; Dodson & Dimitrakopoulos 2009).

The in-plane stress tensor $\boldsymbol{\tau}$ is described by constitutive laws that depend on the material composition of the membrane. In this work, we employ the Skalak *et al.* (1973) law which relates $\boldsymbol{\tau}$'s eigenvalues (or principal elastic tensions τ_β^P, $\beta = 1, 2$) with the principal stretch ratios λ_β by

$$\tau_1^P = \frac{G_s \lambda_1}{\lambda_2}\{\lambda_1^2 - 1 + C\lambda_2^2[(\lambda_1\lambda_2)^2 - 1]\}. \tag{2.4}$$

Note that the reference shape of the elastic tensions is the spherical quiescent shape of the capsule while to calculate τ_2^P reverse the λ_β subscripts.

In (2.4), G_s is the membrane's shear modulus while the dimensionless parameter C is associated with the scaled area-dilatation modulus G_a of the membrane. In particular, the analysis of Barthès-Biesel *et al.* (2002) in the limit of small deformations shows that the area-dilatation modulus is $G_a = G_s(1 + 2C)$; given that the two moduli G_a and G_s take on positive values, this means that $C \geqslant -0.5$. By increasing the parameter C from small values, the tensions superlinear increase with the membrane extension becomes larger (Barthès-Biesel *et al.* 2002), and thus the strain-hardening nature (i.e. the hardness) of a Skalak capsule is increased.

The numerical solution of the interfacial problem described by (2.1)–(2.4) is achieved through our membrane spectral boundary element method which has been employed for the study of the capsule dynamics in strong extensional flows

(Dodson & Dimitrakopoulos 2008, 2009) and in microfluidic channels (Kuriakose & Dimitrakopoulos 2011, 2013; Park & Dimitrakopoulos 2013). Briefly, each boundary is divided into a moderate number of surface elements which are parameterized by two variables ξ and η on the square interval $[-1, 1]^2$. The geometry and physical variables are discretized using Lagrangian interpolation in terms of these parametric variables. The basis points (ξ_i, η_i) for the interpolation are chosen as the zeros of orthogonal polynomials of Gauss type. This is equivalent to an orthogonal polynomial expansion and yields the spectral convergence associated with such expansions. Owing to its spectral nature, our interfacial algorithm has the significant advantage of the accurate determination of any interfacial property, including geometric derivatives and membrane tensions. This is an important issue for the correct and accurate determination of very deformed capsule shapes made from membranes obeying non-linear elastic laws such as the Skalak and Mooney–Rivlin laws, as we discussed in our earlier publication (Dodson & Dimitrakopoulos 2009). The interested reader is referred to our earlier papers for more details on our spectral algorithm (including its spectral accuracy and convergence studies) and the extensional dynamics of strain-hardening and strain-softening capsules (Dodson & Dimitrakopoulos 2008, 2009).

Owing to the specific symmetry of the planar extensional flow, at steady state there is no flow inside the capsule and thus the steady-state overall capsule properties are independent of the viscosity ratio λ. For the same reason, the membrane viscosity (if any), which is not accounted in our computations, does not affect the capsule's steady-state properties (e.g. Lac *et al.* 2004; Dodson & Dimitrakopoulos 2009). Therefore, the steady-state capsule dynamics studied in this work depends on two dimensionless parameters, the capillary number $Ca = \mu G a / G_s$ and the membrane hardness C. In this study, the characteristic length a is used as the length scale and thus curvatures are scaled with a^{-1}, while the membrane tensions are scaled with G_s.

3. Effects of membrane hardness on the capsule steady-state properties

We present now the steady-state properties of a strain-hardening Skalak capsule in a planar extensional flow as a function of the capillary number Ca or the capsule length L_c for different values of membrane hardness, i.e. for $C = 0.1, 0.5, 1, 5$. Whenever our figures present capsule properties with respect to the capsule length L_c, we also include our results for the (strain-softening) neo-Hookean capsule for comparison reasons. As described in our earlier study (Dodson & Dimitrakopoulos 2009), the neo-Hookean capsule is able to reach very deformed steady-state shapes in extensional flows but at much lower flow rates Ca owing to their strain-softening nature. To facilitate the results presentation, in the figures the scales of the variables are omitted and thus the default scales are assumed, i.e. the characteristic length a is used as the length scale while the membrane tensions are scaled with G_s.

Figure 1 shows that for a given flow rate Ca, the capsule extensional deformation increases (i.e. its length L_c increases while its width S_c decreases) as the membrane hardness decreases owing to the less strain-hardening nature of the lower C membranes. Owing to volume preservation, the capsule depth W_c decreases with the membrane hardness C to accommodate the variation of the rest two capsule dimensions. The strong strain-hardening nature of the capsules with $C \geqslant 0.5$ enable them to withstand increased flow rates and thus reach very elongated shapes, e.g. shapes with $L_c/a \approx 4$ for $Ca = 5$.

It is of interest to note that in figure 1 we do not present results for very low flow rates Ca. In this case, near steady state, compressive tensions are developed

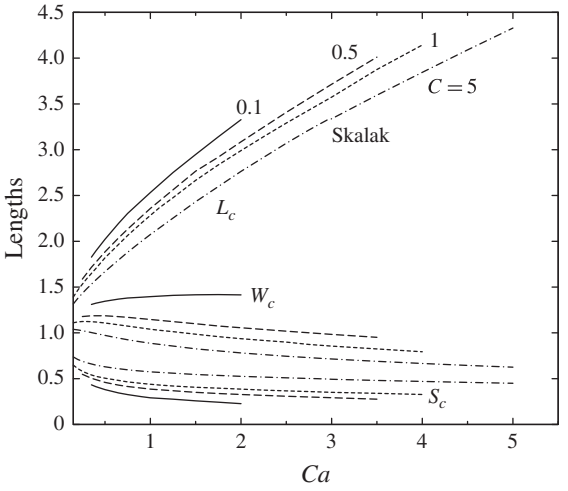

FIGURE 1. Steady-state capsule's half-lengths L_c, S_c and W_c in the x, y and z directions as a function of the capillary number Ca for a Skalak capsule with $C = 0.1, 0.5, 1, 5$ in a planar extensional flow. Note that for a given capsule shape, we determine the three capsule dimensions, L_c, S_c and W_c, as the half of the maximum distance of the capsule surface in the x, y and z coordinates, respectively, by employing a Newton method to solve the optimization problems using the spectral discretization points on the membrane.

on the capsule membrane resulting in wrinkling around the capsule equator and interfacial breaking for computational algorithms without sufficient bending resistance, as identified via the bi-cubic B-spline method of Lac *et al.* (2004) and verified later via our spectral boundary element method (Dodson & Dimitrakopoulos 2008, 2009). Lac *et al.* (2004) also studied the influence of the membrane hardness on the deformation of Skalak capsules. However, owing to interfacial breaking, their results were restricted to only moderate flow rates and deformations, i.e. capillary numbers up to $Ca = 0.4, 0.6, 1.35$ (or capsule lengths $L_c/a \lesssim 2$) for membrane hardness $C = 0.5, 1, 10$, respectively. Our study shows that the failure of the (low-order) bi-cubic B-spline method of Lac *et al.* (2004) at higher flow rates in planar extensional flows was a numerical artifact and not of physical origin, as also discussed in our earlier publication (Dodson & Dimitrakopoulos 2009). It is interesting to mention that the high-order algorithm of Walter *et al.* (2010) was also able to reach large steady-state deformations for capsules in strong planar extensional flows, while their results for the interfacial shape of Skalak $C = 1$ capsules up to $Ca = 3$ are in excellent agreement (i.e. for at least three significant digits) with the findings from our spectral algorithm (Dodson & Dimitrakopoulos 2009). Note that, in contrast to our spectral algorithm, the algorithm of Walter *et al.* (2010) contains small bending resistance, and thus the findings agreement verifies that small bending resistance cannot affect the capsule's overall shape (Chang & Olbricht 1993*a*; Pieper *et al.* 1998; Rachik *et al.* 2006).

To identify better the variation of the capsule dimensions with its extension, in figure 2 we present the capsule width and depth as a function of its length. As the capsule length L_c increases in stronger flows, all capsules become thinner while the capsule width S_c increases monotonically with the strain-hardening of the membrane. More interestingly, the variation of the capsule depth W_c with its extension L_c depends on the degree of the membrane strain-hardening; the less-strain-hardening capsules

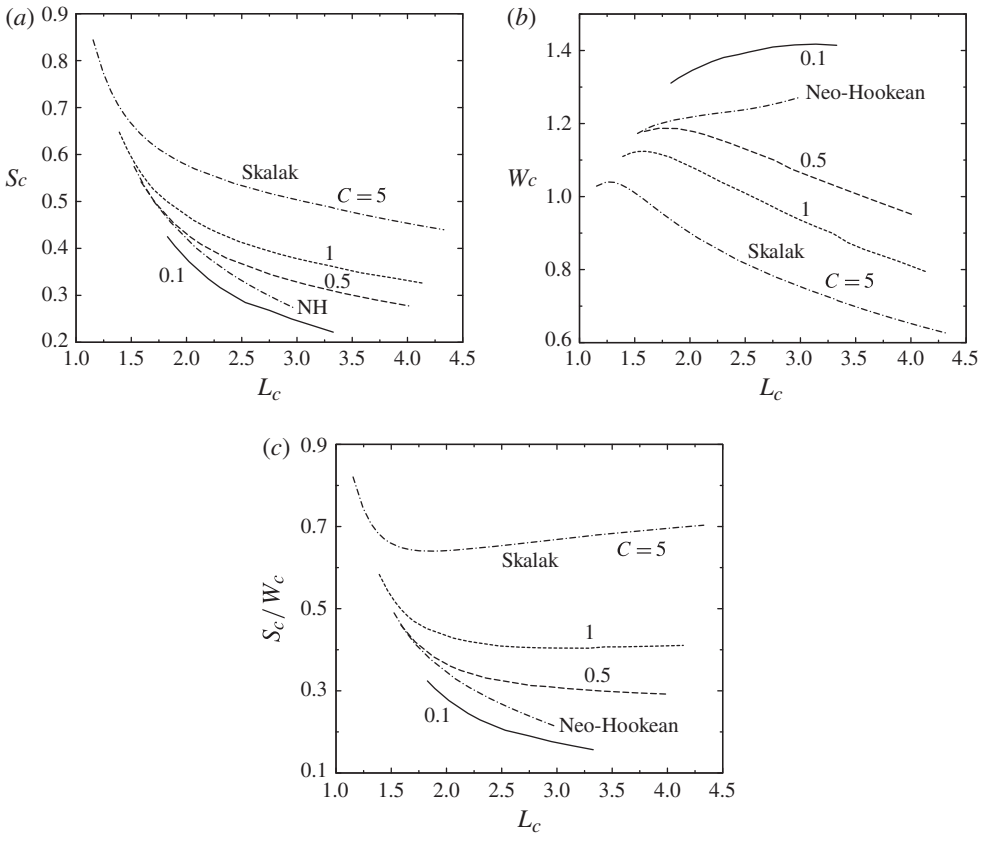

FIGURE 2. Steady-state capsule's dimensions as a function of its length L_c for a neo-Hookean (NH) and a Skalak capsule with $C = 0.1, 0.5, 1, 5$ in a planar extensional flow: (*a*) width S_c, (*b*) depth W_c and (*c*) ratio S_c/W_c.

(such as the Skalak $C = 0.1$ and neo-Hookean capsules) become flatter while the depth of the more-strain-hardening capsules (e.g. $C \geqslant 0.5$) decreases with elongation. To investigate more the behaviour of capsule's lateral dimensions with elongation, in figure 2(*c*) we plot the width-to-depth ratio S_c/W_c. This figure shows that the width-to-depth ratio S_c/W_c of the more-strain-hardening capsules ($C \geqslant 0.5$) reaches an (approximately) constant value at higher elongations while the less-strain-hardening $C = 0.1$ capsule and the strain-softening neo-Hookean capsule become increasingly lamellar with extension.

For a better view of the effects of membrane hardness on the capsule dimensions, in figure 3 we present three-dimensional views of a Skalak capsule with $C = 0.1, 0.5, 5$ in moderately strong flows with $Ca = 1, 1.2, 1.5$, respectively, where all capsules have nearly the same length, $L_c/a \approx 2.5$. As the membrane hardness C increases, the capsule depth W_c decreases and its cross-section becomes more rounded, while all capsules have obtained pointed edges.

In figure 4 we present three-dimensional views of a Skalak capsule with $C = 0.1, 0.5, 5$ in a planar extensional flow with $Ca = 2, 3.5, 5$, respectively. These flow rates represent the highest Ca for which we determined steady-state shapes for the associated membrane hardness C. Observe that the less-strain-hardening Skalak

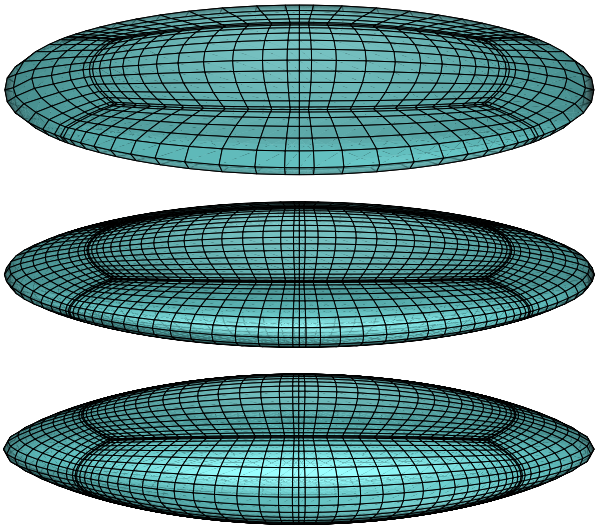

FIGURE 3. (Colour online) Steady-state shape of a Skalak capsule with $C = 0.1, 0.5, 5$ in a planar extensional flow with $Ca = 1, 1.2, 1.5$, respectively. All capsules have nearly the same length ($L_c/a \approx 2.5$) while the shapes are plotted as seen slightly askew from the positive z-axis to reveal the capsule's depth.

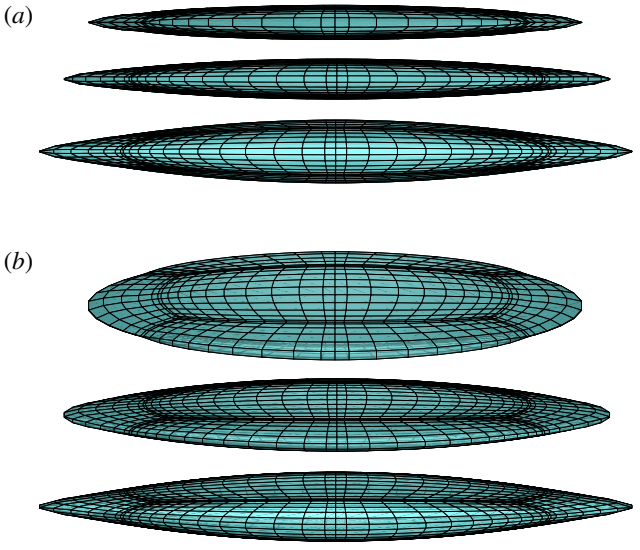

FIGURE 4. (Colour online) Steady-state shape of a Skalak capsule with $C = 0.1, 0.5, 5$ in a planar extensional flow with $Ca = 2, 3.5, 5$, respectively. The capsule shape is plotted as seen from the positive z-axis in (a) and slightly askew from this axis in (b) to reveal the capsule depth.

capsule with $C = 0.1$ becomes very flat in the lateral direction (i.e. it becomes lamellar) with flat and very pointed edges that result in interfacial breaking for $Ca > 2$ owing to the computational difficulty in determining accurately these shapes. On the other hand, the more-strain-hardening Skalak capsules with $C = 0.5, 5$ reach

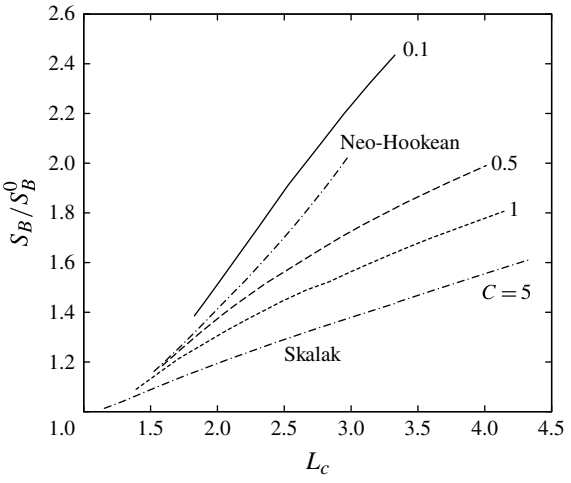

FIGURE 5. Steady-state surface area S_B of the capsule (scaled by the surface area S_B^0 of the reference spherical shape) as a function of the capsule length L_c, for a neo-Hookean and a Skalak capsule with $C = 0.1, 0.5, 1, 5$ in a planar extensional flow.

large steady-state extensions in much higher flow rates with a rounded cross-section while we have not found an upper Ca limit in the existence of steady-state shapes.

It is of interest to note here that our computations show that the lamellar shape of Skalak capsules with $C \leqslant 0$ becomes very flat with pointed edges in both the flow and the lateral directions owing to the very weak strain-hardening nature of these membranes. Such shapes are very difficult to be computed numerically, i.e. we are only able to determine very limited steady-state shapes of these capsules and thus they are not included in the present study.

The overall capsule deformation can also be characterized via the evolution of its surface area S_B. Our computational results show that the capsule's surface area S_B increases with the flow rate Ca in a manner similar to that for the capsule length L_c depicted earlier in figure 1, and thus the surface area S_B shows a nearly linear increase with the capsule length L_c as seen in figure 5. Owing to their lamellar shape, the less-strain-hardening capsules (such as the Skalak $C = 0.1$ and neo-Hookean capsules) show a significant surface-area increase at large elongations, e.g. the surface area of the Skalak $C = 0.1$ capsule increases to nearly 140 % when $L_c = 3.3$. The surface-area increase with the capsule elongation is much smaller for the more-strain-hardening capsules owing to their more circular cross-section (or higher S_c/W_c ratio) shown earlier in figure 2(*c*), e.g. the surface area of the Skalak $C = 5$ capsule increases to 60 % only when $L_c = 4.3$.

Another property associated with the capsule's overall deformation is the maximum membrane tension. Figure 6(*a*) reveals that the maximum principal tension τ_{max}^P at steady state increases monotonically with the flow rate Ca and thus with the capsule deformation. In addition, the capsules with smaller hardness C are associated with higher membrane tensions at a given capillary number, owing to their less-strain-hardening nature which results in a higher interfacial deformation at a given flow rate. Replotting our τ_{max}^P data with respect to the capsule length L_c in figure 6(*b*), the strain-hardening nature of the Skalak capsules is clearly revealed. The effects of the membrane hardness C are now limited and the curves for the different

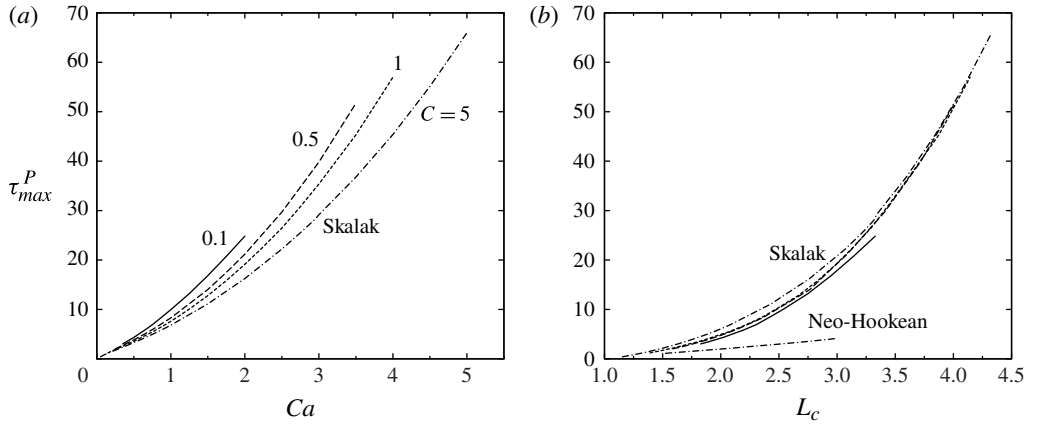

FIGURE 6. Steady-state maximum principal tensions τ^P_{max} among the spectral discretization points on the membrane as a function of (*a*) the capillary number Ca and (*b*) the capsule's length L_c, for a neo-Hookean and a Skalak capsule with $C = 0.1, 0.5, 1, 5$ in a planar extensional flow.

Skalak capsules nearly coincide and separate from that of the neo-Hookean capsule which requires significantly lower membrane tensions τ^P_{max} for a given elongation L_c owing to its strain-softening nature. It is of interest to note that the maximum tension at steady state occurs at the intersection of the capsule's surface with the z-axis (i.e. the location of the maximum capsule depth W_c) and always points in the direction of the capsule's elongation. Thus, this location is the most probable to rupture due to excessive tensions in extensional flows.

We now turn our attention to the capsule pointed edges where the smallest interfacial length scales occur. To describe the capsule edges, including the local length scales there, in figure 7 we present the edge curvatures $\mathscr{C}_{xy}$ and $\mathscr{C}_{xz}$ as a function of capsule's extension L_c. Observe that both $\mathscr{C}_{xy}$ and $\mathscr{C}_{xz}$ are line curvatures, determined along the interfacial cross-section with the $z = 0$ and $y = 0$ planes, respectively, while they take on positive values for the spherical quiescent shape of the capsule where $\mathscr{C}_{xy} = \mathscr{C}_{xz} = a^{-1}$.

The dependence of the edge curvature $\mathscr{C}_{xy}$ (which represents the sharper edge profile and thus the smaller local length scale) presented in figure 7(*a*) is similar to that identified in our earlier study for the Skalak $C = 1$ capsules (Dodson & Dimitrakopoulos 2009). For all capsule hardness, this edge curvature shows a very fast (exponential-like) increase with the capsule elongation L_c which is higher for the less-strain-hardening capsules (such as the Skalak $C = 0.1$ and neo-Hookean capsules) owing to their lamellar shape. It is of interest to note that Higley, Siegel & Booty (2012) also found that the steady-state edge curvature of Hookean two-dimensional capsules increases exponentially with the flow rate in extensional flows. This suggests that the existence of a very small (in particular, exponentially small) edge length scale is a general feature of capsules in strong extensional flows, facilitated by the development of very small membrane tensions at the capsule tips (Dodson & Dimitrakopoulos 2008, 2009; Higley *et al.* 2012).

Figure 7(*b*) shows the elongation dependence of the edge curvature $\mathscr{C}_{xz}$ that characterizes the local edge length scale along the lateral z-axis. For the less-strain-hardening capsules, this edge curvature remain small (i.e. $\leqslant 5$) but for the

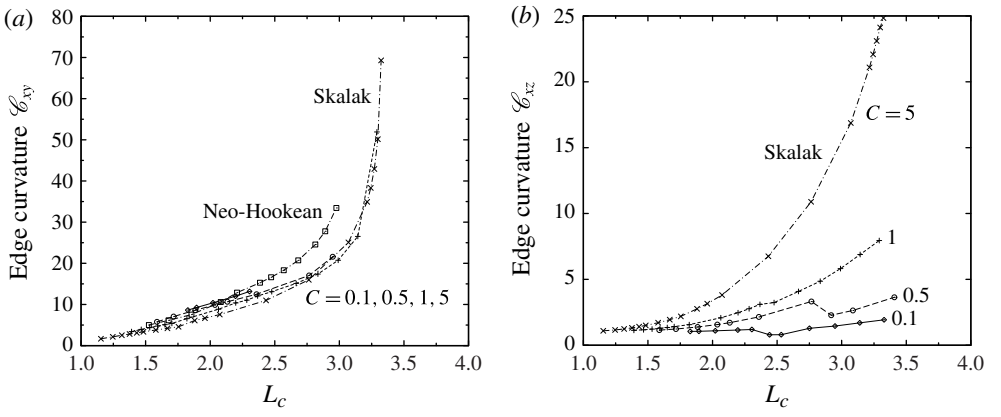

FIGURE 7. Steady-state edge curvature as a function of capsule's length L_c for a neo-Hookean and a Skalak capsule with $C = 0.1, 0.5, 1, 5$ in a planar extensional flow. (*a*) Edge curvature $\mathscr{C}_{xy}$ determined along the interfacial cross-section with the $z = 0$ plane. (*b*) Edge curvature $\mathscr{C}_{xz}$ determined along the interfacial cross-section with the $y = 0$ plane. In (*b*) the neo-Hookean curve lies between the curves for $C = 0.1$ and $C = 0.5$ and has been omitted for clarity.

most-strain-hardening capsules (such as the Skalak $C = 5$ capsule) this edge curvature increases fast with elongation, reaching about half the curvature $\mathscr{C}_{xy}$.

Therefore, less-strain-hardening capsules are characterized by only a small local length scale at their edges (i.e. that along the $z = 0$ profile) owing to their lamellar shape. On the other hand, strong-strain-hardening capsules are characterized by two small local length scales at their edges (of similar magnitude) owing to their slender spindle shape.

The steady-state deformation results for the overall capsule shape we provide in this section can be used to identify the elastic properties of a capsule's membrane, by comparing our computation data with experimental measurements of the capsule dimensions at planar extensional flows. These experiments can be performed in classical or microfluidic four-roll mill devices (Bentley & Leal 1986; Ha & Leal 2001; Hudson *et al.* 2004), in order to provide measurements of the capsule's length L_c and width S_c in different flow rates G. In this case, a comparison of our computation data with experimental measurements can reveal both the shear modulus G_s and the area-dilatation modulus G_a of a strain-hardening capsule. To explain this, observe that for a given capsule length L_c, figure 2(*a*) shows that the capsule width S_c is a monotonic function of the membrane hardness C, and thus this comparison can reveal the membrane hardness C. Knowing the membrane hardness C and the capsule's length L_c (or width S_c), a comparison of the experimental measurements with our computation data shown in figure 1 reveals the appropriate capillary number Ca and thus the membrane's shear modulus G_s. This procedure has the advantage of not depending on, or being influenced by, the fluids' viscosity ratio or the membrane viscosity (if any).

It is of interest to note that the early study of Chang & Olbricht (1993*a*) utilized the capsule investigation in four-roll mill extensional flows as a methodology to determine the membrane's Young modulus (which is a function of both shear and area-dilatation moduli). To achieve this, the authors compared with asymptotic theories the experimental measurement of the capsule's length L_c and width S_c in the form

of the deformation parameter $D \equiv (L_c - S_c)/(L_c + S_c)$ at low flow rates Ca. Our study reveals that a comparison of the same kind of experimental measurements at moderate and high flow rates with our computational results can reveal both the shear and area-dilatation moduli. Observe that the proposed determination of both membrane moduli via a single experimental technique (instead of the commonly required two different experiments; see e.g. Pieper *et al.* (1998) and Koleva & Rehage (2012)) relies on two properties. First, we utilize both the length L_c and width S_c of the capsule, and not the single deformation parameter D which reduces the two degrees of freedom into one. Second, we propose investigation in moderate and high flow rates where the effects of the membrane hardness C become prominent and thus capsules with different area-dilatation modulus can be identified.

4. Scaling analysis for the steady-state capsule dynamics

In this section we provide a scaling analysis for the steady-state dynamics of strain-hardening capsules in strong planar extensional flows. First, we describe our analysis for the more strain-hardening Skalak capsules with $C \geqslant 0.5$ studied in this work. This analysis is later modified to be valid for the lamellar Skalak $C = 0.1$ capsules in planar extensional flows. To facilitate the results presentation, in the figures the scales of the variables are omitted and thus the default scales are assumed, i.e. the characteristic length a is used as the length scale while the membrane tensions are scaled with G_s.

4.1. *Scaling analysis for slender spindle-like capsules*

Our first analysis is based on the similar scaling analysis of Acrivos (1983) for slender bubbles in strong axisymmetric extensional flows which has been proved to be also valid for slender bubbles in planar extensional flows even though the bubble shape in these flows becomes significantly non-axisymmetric (see e.g. Hinch & Acrivos 1979). We emphasize that owing to the specific symmetry of the planar extensional flow, at steady state there is no flow on the interfacial membrane or inside the capsule, and thus the capsule dynamics in planar extensional flows corresponds better to the dynamics of low-viscosity drops (or bubbles) as also discussed in our earlier papers (Dodson & Dimitrakopoulos 2008, 2009). Our capsule analysis is more complicated than the corresponding scaling analysis of Acrivos (1983) for bubbles with a constant surface tension γ, owing to the fact that the capsule tensions grow with its deformation and, in particular, they are a nonlinear function of the local stretch ratios as seen in (2.4). Nevertheless, we are able to derive (closed) predictions without the need to utilize information from our computational findings while these predictions provide useful physical insight on the extensional capsule dynamics.

Considering a strain-hardening Skalak capsule with $C \geqslant 0.5$ in a strong planar extensional flow, its steady-state cross-section becomes elliptical and thus the capsule width S_c is smaller than its depth W_c, as discussed in § 3. However, in strong flows (or large elongations), the ratio S_c/W_c is practically constant as shown in figure 2(*c*), and thus $S_c \sim W_c$. For these capsules, volume preservation requires that

$$V \sim a^3 \sim L_c\, W_c^2 \quad \text{or} \quad \frac{W_c}{a} \sim \left(\frac{L_c}{a}\right)^{-1/2}. \tag{4.1}$$

It is of interest to note that this geometric constraint justifies the fact that these capsules become slender with elongation at high flow rates as shown in figure 2.

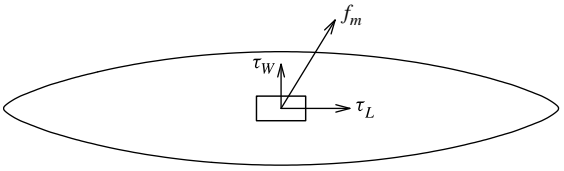

FIGURE 8. The interfacial deformation creates elongation and lateral tensions, denoted as τ_L and τ_W, locally on the capsule membrane. Both tensions contribute to the restoring membrane normal stress f_m.

The steady-state capsule dynamics is associated with the balance on the capsule membrane of the deforming flow normal stress and the restoring membrane normal stress, owing to the curvature term in (2.3). Since a planar extensional flow mainly impacts the capsule on its top and bottom surfaces (i.e. along the positive or negative y-axis), the most appropriate membrane location to enforce the stress balance is the location of capsule's maximum width S_c, i.e. the centre of the capsule's top or bottom surface. Observe that this location is characterized by two dimensions, i.e. the capsule length L_c and its depth W_c.

In a strong extensional flow, the deforming normal stress of the external fluid exerted on the capsule membrane is

$$f_\mu \sim \mu G \tag{4.2}$$

and results only from the external pressure since the viscous normal stress is identically zero on the capsule interface at steady state owing to the membrane immobilization. As seen in the second term on the right-hand side of (2.3), the restoring membrane normal stress is the sum of the two principal membrane stresses (along the flow direction denoted by the subscript L and along the lateral direction of the capsule depth denoted by the subscript W), i.e.

$$f_m \sim \tau_L G_s \mathscr{C}_L + \tau_W G_s \mathscr{C}_W \sim \frac{\tau_L G_s}{L_c} + \frac{\tau_W G_s}{W_c}, \tag{4.3}$$

where $\mathscr{C}_L$ and $\mathscr{C}_W$ denote the interfacial curvature along the flow and the lateral directions, respectively. Note that the dimensionless tensions τ_L and τ_W account for the tension development in the corresponding direction owing to the interfacial deformation, as illustrated in figure 8. Steady-state dynamics implies a balance of the two opposite normal stresses on the membrane, i.e.

$$f_\mu \sim f_m \quad \text{or} \quad \mu G \sim \frac{\tau_L G_s}{L_c} + \frac{\tau_W G_s}{W_c}, \tag{4.4}$$

and, thus,

$$Ca = \frac{\mu G a}{G_s} \sim \frac{\tau_L}{L_c/a} + \frac{\tau_W}{W_c/a}. \tag{4.5}$$

To proceed we need to find the scaling of the two principal tensions τ_L and τ_W. For this, we utilize the Skalak *et al.* law, given by (2.4), by approximating the principal stretch ratios with the corresponding capsule lengths, i.e.

$$\lambda_1 \approx \frac{L_c}{a} \quad \text{and} \quad \lambda_2 \approx \frac{W_c}{a}. \tag{4.6}$$

Simple algebra reveals that

$$\tau_L \sim \left(\frac{L_c}{a}\right)^{3.5} + C\left(\frac{L_c}{a}\right)^{1.5} \sim \left(\frac{L_c}{a}\right)^{3.5} \tag{4.7}$$

and

$$\tau_W \sim -\left(\frac{L_c}{a}\right)^{-1.5} + C\left(\frac{L_c}{a}\right)^{1.5} \sim C\left(\frac{L_c}{a}\right)^{1.5}. \tag{4.8}$$

Observe that our analysis predicts that, for elongated capsules with large enough L_c, the strong elongation tension τ_L of the capsules studied in this work ($0.5 \leqslant C \leqslant 5$) results mainly from the membrane's shearing resistance to the capsule elongation while it is not affected much by the membrane's area-dilatation resistance. (The area-dilatation resistance can still contribute significantly at high enough membrane hardness, i.e. for $C \gg L_c/a$.) In addition, the weaker lateral tension τ_W is shown to result mainly from the membrane's area-dilatation resistance and, thus, for a given capsule length L_c, it increases with the membrane hardness C.

Based on the scaling of the two directional tensions and of the capsule's depth, given by (4.1), the normal stress balance represented by (4.5) gives

$$Ca \sim \left(\frac{L_c}{a}\right)^{2.5} + C\left(\frac{L_c}{a}\right)^{2}. \tag{4.9}$$

Observe that the first term in the right-hand-size of (4.9) results from the elongation tension normal stress while the second term results from the lateral tension normal stress. Therefore our analysis suggests that both the strong elongation tension τ_L and the weaker lateral tension τ_W participate in the steady-state dynamics by producing restoring normal stresses owing to the corresponding curvatures. For small and moderate values of the membrane hardness C, as the ones employed in this work, we expect the elongation tension normal stress τ_L/L_c to dominate the stabilizing dynamics. However, for very large membrane hardness $C \gg 1$, our analysis predicts that the lateral tension normal stress τ_W/W_c should dominate the restoring tension forces.

To be able to compare the predictions of our scaling analysis with our computations, we determined computationally the tensions τ_L^y and τ_W^y as the principal tensions at the middle of the capsule's top surface (i.e. at the location of the maximum width S_c along the positive y-axis) for Skalak capsules with $C = 0.5, 5$. For both capsules, our computations show that the capillary number Ca as a function of the capsule elongation L_c follows the scaling of the elongation tension normal stress τ_L^y/L_c, i.e. the deforming flow normal stress is mainly balanced by the elongation tension normal stress.

In addition, least-squares fitting of our computational results for capsule length $L_c/a \geqslant 2$ shows that for the Skalak $C = 0.5$ the elongation tension and the capillary number grow as

$$\tau_L \sim \left(\frac{L_c}{a}\right)^{3.40\pm0.04} \quad \text{and} \quad Ca \sim \left(\frac{L_c}{a}\right)^{2.34\pm0.06}. \tag{4.10}$$

Both findings are in good agreement with the predictions of our scaling analysis, i.e. with (4.7) and (4.9) for large enough L_c,

$$\tau_L \sim \left(\frac{L_c}{a}\right)^{3.5} \quad \text{and} \quad Ca \sim \left(\frac{L_c}{a}\right)^{2.5} \tag{4.11}$$

as also shown in figure 9 for τ_L^y and Ca.

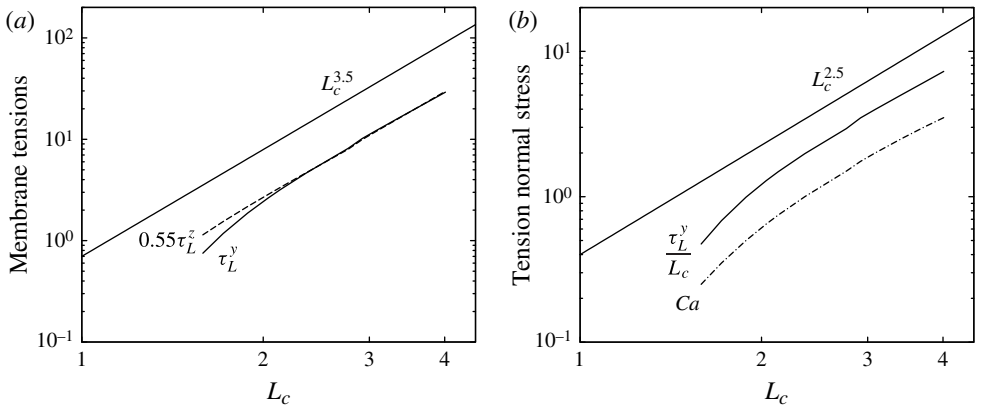

FIGURE 9. (*a*) Steady-state elongation membrane tensions τ_L^y and τ_L^z as a function of the capsule's length L_c in a log–log plot for a Skalak capsule with $C = 0.5$ in a planar extensional flow. Also shown as a heavy line is the curve $L_c^{3.5}$. (*b*) As in (*a*) but for the tension normal stress τ_L^y/L_c and the capillary number Ca as a function of the capsule's length L_c. Also shown as a heavy line is the curve $L_c^{2.5}$.

For the Skalak $C = 5$ capsule, least-squares fitting of our computational results for capsule length $L_c/a \geqslant 1.67$ reveal that the elongation tension and the capillary number increase as

$$\tau_L \sim \left(\frac{L_c}{a}\right)^{3.1\pm0.01} \quad \text{and} \quad Ca \sim \left(\frac{L_c}{a}\right)^{2.1\pm0.04} \tag{4.12}$$

as shown in figure 10, which is slightly slower than that predicted via our scaling analysis in (4.11). We emphasize that even though the actual power of growth, i.e. 2.1 ± 0.04, is closer to that predicted based on the lateral tension normal stress, see the last term of (4.9), our computations show that even for $C = 5$ the deforming flow normal stress is mainly balanced by the elongation tension normal stress. Thus, the reduced power of growth for the $C = 5$ capsules does not denote distinct physics but only a difference between the scaling predictions and the actual computations.

Our scaling analysis helps to understand the reason for the appearance of the maximum tension at the location of the maximum capsule depth W_c, and not the location of the maximum capsule width S_c which may be an obvious guess. To explain this, we note that our analysis for the capsule tensions shown in (4.7) and (4.8) is also applicable on the capsule's front or back surface (i.e. the capsule surface along the positive or negative z-axis) since $S_c \sim W_c$. By utilizing that the lateral stress ratio λ_2 is $\lambda_2 \approx W_c/a$ along the direction of the capsule depth and $\lambda_2 \approx S_c/a$ along its width, our tension analysis for τ_L seen in (4.7) predicts that

$$\frac{\tau_L^y}{\tau_L^z} \sim \frac{S_c}{W_c} \tag{4.13}$$

owing to the denominator of λ_2 in the Skalak *et al.* law, given by (2.4), i.e. the fact that $\tau_L \sim \lambda_2^{-1}$. This explains why the maximum tension $\tau_{max}^P \equiv \tau_L^z$ on the capsule membrane is located at the point of the maximum capsule depth W_c, i.e. the middle of the capsule's front or back surface. Based on the values of the ratio S_c/W_c shown in figure 2(*c*), our scaling analysis predicts that $\tau_L^y/\tau_L^z \approx 0.3, 0.7$ for a Skalak capsule with $C = 0.5, 5$ respectively, while our computational results show that $\tau_L^y/\tau_L^z \approx 0.55, 0.94$, as seen in figure 9(*a*) and 10(*a*).

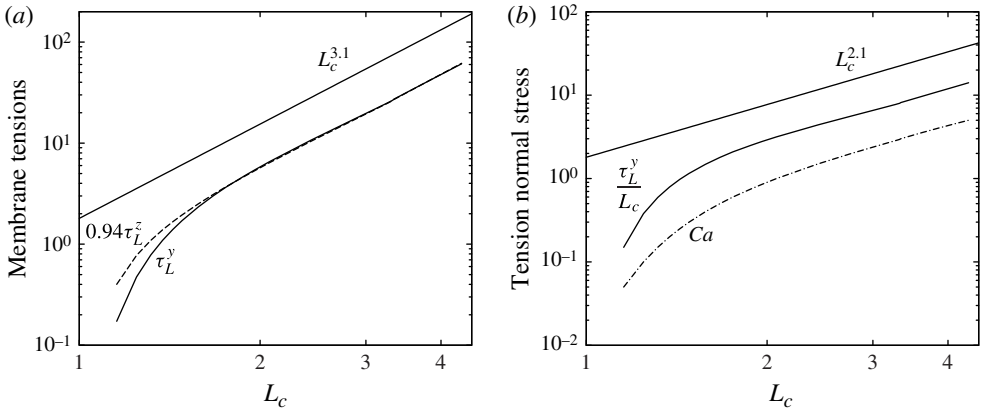

FIGURE 10. (*a*) Steady-state elongation membrane tensions τ_L^y and τ_L^z as a function of the capsule's length L_c in a log–log plot for a Skalak capsule with $C = 5$ in a planar extensional flow. Also shown as a heavy line is the curve $L_c^{3.1}$. (*b*) As in (*a*) but for the tension normal stress τ_L^y/L_c and the capillary number Ca as a function of the capsule's length L_c. Also shown as a heavy line is the curve $L_c^{2.1}$.

4.2. *Comparison with bubbles dynamics*

For slender bubbles in strong axisymmetric extensional flows, the scaling analysis of Acrivos (1983) predicts that the normal flow stress on the bubble interface is $f_\mu \sim \mu G$ (owing to both the pressure and the viscous stress in the external fluid) while the restoring surface tension force is $f_m \sim \gamma/W_c$, i.e. it results from the capsule's lateral direction only, since the bubble surface tension γ is constant while the volume preservation predicts again that $W_c/a \sim (L_c/a)^{-1/2}$. Balancing of these opposite stresses produces

$$Ca_d \sim \left(\frac{L_c}{a}\right)^{0.5} \quad \text{or} \quad \frac{L_c}{a} \sim Ca_d^2 \tag{4.14}$$

as derived by Acrivos (1983), which shows that for a given capillary number $Ca_d = \mu Ga/\gamma$ or $Ca = \mu Ga/G_s$, bubbles elongate more than the strain-hardening capsules in an extensional flow since they have a constant surface tension γ while the membrane tensions grow significantly with the capsule deformation.

4.3. *Scaling analysis for lamellar capsules*

Our scaling analysis can also be modified to be valid for the lamellar Skalak $C = 0.1$ capsule in a planar extensional flow. As shown in figures 1 and 2(*b*), the depth W_c of this capsule has been increased from its quiescent value at low flow rates. However, at the large elongations of interest in this study, the capsule depth W_c varies little, and thus can be regarded as constant, i.e. $W_c = O(a)$. In this case, volume preservation of the lamellar capsule requires that

$$V \sim a^3 \sim L_c\, W_c\, S_c \quad \text{or} \quad \frac{S_c}{a} \sim \left(\frac{L_c}{a}\right)^{-1}. \tag{4.15}$$

It is of interest to note that this geometric constraint justifies the faster width reduction of the lamellar capsule with the elongation L_c, compared with that of the more-strain-hardening spindle-like capsules with $C \geqslant 0.5$, as shown in figure 2.

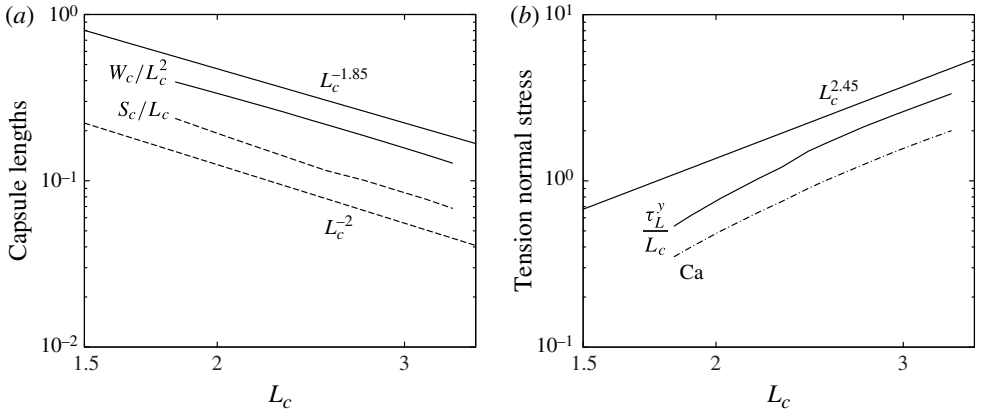

FIGURE 11. (*a*) Steady-state capsule's width S_c/L_c and depth W_c/L_c^2 as a function of its length L_c in a log–log plot for a Skalak capsule with $C = 0.1$ in a planar extensional flow. Also shown as heavy lines are the curves $L_c^{-1.85}$ and L_c^{-2}. (*b*) As in (*a*) but for the tension normal stress τ_L^y/L_c and the capillary number Ca as a function of the capsule's length L_c. Also shown as a heavy line is the curve $L_c^{2.45}$.

While we can employ the length scale $W_c = O(a) \sim L_c^0 a$ in our analysis, a more accurate description can be achieved if we use the exact relationship of the capsule depth W_c with its length L_c from our computations. As shown in figure 11(*a*), least-squares fitting of our computational results reveals that

$$\frac{W_c}{L_c^2/a} \sim \left(\frac{L_c}{a}\right)^{-1.85\pm0.01} \quad \text{or} \quad \frac{W_c}{a} \sim \left(\frac{L_c}{a}\right)^{0.15}. \tag{4.16}$$

Approximating again the principal stretch ratios with the corresponding capsule lengths as in (4.6), the Skalak *et al.* law (2.4) predicts that the elongation tension (which produces again the dominant tension normal stress) is now

$$\tau_L \sim \left(\frac{L_c}{a}\right)^{2.85} + C\left(\frac{L_c}{a}\right)^{3.45} \sim C\left(\frac{L_c}{a}\right)^{3.45} \tag{4.17}$$

i.e. it results mainly from the membrane area-dilatation resistance for large enough L_c. Therefore, for the lamellar Skalak $C = 0.1$ capsule, the normal stress balance, given by (4.5), results in

$$Ca \sim \frac{\tau_L}{L_c/a} \sim C\left(\frac{L_c}{a}\right)^{2.45}. \tag{4.18}$$

Both the scaling for the elongation tension τ_L shown in (4.17) and that for the capillary number shown in (4.18) are in good agreement with our computational results as seen in figure 11(*b*). In particular, least-squares fitting of our computational results for capsule length $L_c/a \geqslant 2.23$ reveal that the elongation tension and the capillary number increase as

$$\tau_L \sim \left(\frac{L_c}{a}\right)^{3.47\pm0.05} \quad \text{and} \quad Ca \sim \left(\frac{L_c}{a}\right)^{2.50\pm0.05}. \tag{4.19}$$

We note that if we utilize the simple depth scaling $W_c = O(a) \sim L_c^0 a$, our analysis predicts that

$$Ca \sim \frac{\tau_L}{L_c/a} \sim (1+C)\left(\frac{L_c}{a}\right)^2 \tag{4.20}$$

which is not as accurate as the prediction based on the exact depth–length relationship.

5. Discussion

In this paper we have investigated computationally the steady-state dynamics of an elastic capsule in moderate and strong planar extensional flows. In particular, we have considered an elastic capsule made of a strain-hardening membrane (following the Skalak *et al.* constitutive law) with varying area-dilatation resistance (compared with its shearing resistance) in order to investigate the effects of membrane hardness C.

We emphasize that high flow rates are commonly encountered in industrial and physiological processes. For example, for millisize capsules made from amino-methacrylate membranes with shear modulus $G_s = O(10^{-2})$ N m^{-1}, flow rates $Ca = O(1)$ require shear stress $\mu G = O(10)$ Pa (Pieper *et al.* 1998); these flow rates require shear stress $\mu G = O(1)$ Pa for microcapsules with similar size and shear modulus as those of the erythrocyte, i.e. $a = 2.8$ μm and $G_s = O(10^{-6})$ N m^{-1} (Popel & Johnson 2005; Dimitrakopoulos 2012). It is of interest to note that the required flow rates for large deformations of millisize and microsize capsules have long been achieved in four-roll mill experiments with droplets and bubbles (with size and fluids/interfacial properties similar to those of the capsules) under Stokes flow conditions (Bentley & Leal 1986; Ha & Leal 2001).

In addition, our work investigates the capsule dynamics up to quite large deformations, i.e. surface-area increases up to 140 % for the less-strain-hardening $C = 0.1$ Skalak capsules and 60 % for the more-strain-hardening $C = 5$ Skalak capsules. This range of membrane deformation has been investigated in compression experiments and the experimental findings have shown that the capsule dynamics can be well described by a single constitutive law with fixed value of the employed moduli (Carin *et al.* 2003; Rachik *et al.* 2006). Thus, our modelling is appropriate for the entire range of deformations we study.

We note that our results were derived for zero bending resistance. As the membrane's bending modulus K_b increases from zero but still remains sufficiently small, it should not affect the capsule's overall shape as long as $K_b/a^2 \ll G_s$, a condition valid for a wide range of capsules as discussed in § 2. Sufficiently small bending resistance is not expected to affect the edge curvature of our elongated capsules as long as $K_b/R_c^2 \ll G_s$, where R_c is the edge's radius of curvature, or roughly when the actual membrane thickness is smaller than the edge's radius of curvature. We emphasize again that the pointed edges of our capsules are in qualitative agreement with experimental findings of polylysine capsules in planar extensional flows (Barthès-Biesel 1991) while these local conformations suggest that the actual polylysine membrane has negligible bending resistance.

Our investigation complements earlier experimental and theoretical studies (Barthès-Biesel & Rallison 1981; Chang & Olbricht 1993*a*; Lac *et al.* 2004; Dodson & Dimitrakopoulos 2008, 2009), and has revealed a number of new physical results and insight for the capsule dynamics in extensional flows.

In particular, as the flow rate increases, strain-hardening capsules with different membrane hardness reach elongated steady-state configurations but the cross-section

of the more strain-hardening capsules preserves its elliptical shape while the less strain-hardening capsules become lamellar, similarly to the strain-softening neo-Hookean capsules we investigated in our earlier work (Dodson & Dimitrakopoulos 2009). The capsule deformation in strong extensional flows is accompanied with very pointed edges, i.e. large edge curvatures and thus small local edge length scales, which makes the current investigation a multi-length interfacial dynamics problem.

The pointed profiles of our shapes are in qualitative agreement with experimental findings on capsules in planar extensional flows (Barthès-Biesel 1991) and resemble very much the elongated and pointed profiles of low-viscosity droplets in planar extensional flows. See, for example, the experimental photos shown in figure 5(*b*) in the work by Taylor (1934) and in figure 27 in the paper by Bentley & Leal (1986). We emphasize again that owing to the specific symmetry of the planar extensional flow, at steady state there is no flow inside the capsule, and thus the capsule dynamics in planar extensional flows corresponds better to the dynamics of low-viscosity drops as also discussed in our earlier papers (Dodson & Dimitrakopoulos 2008, 2009).

Our computational results for slender spindle or lamellar strain-hardening capsules are accompanied with a scaling analysis for each capsule conformation which provides useful physical insight on the extensional capsule dynamics. Even though the membrane tensions grow nonlinearly with the capsule deformation, we are able to derive (closed) predictions for the extensional capsule dynamics by approximating the principal stretch ratios with the corresponding capsule lengths as in (4.6).

Both the more strain-hardening spindle Skalak capsules with $C \geqslant 0.5$ and the lamellar $C = 0.1$ capsules produce practically the same capillary number-elongation relationship, i.e. nearly $Ca \sim (L_c/a)^{2.5}$, that results from the normal stress balance of the deforming external pressure with the dominant restoring elongation tension which scales as nearly $\tau_L \sim (L_c/a)^{3.5}$ for both types of capsules. (See also the similar dependence of the principal tensions τ^P_{max} on the capsule length L_c for all Skalak capsules shown in figure 6(*b*).) However, our scaling analysis shows that the physical origin of the elongation tension is different; for the more-strain-hardening Skalak capsules it results mainly from the membrane's shearing resistance while for the Skalak $C = 0.1$ capsule it results mainly from its area-dilatation resistance, as shown in (4.7) and (4.17). Therefore, in our present computational work we have identified two types of strain-hardening steady-state extensional dynamics associated with the two distinct capsule conformations we found, i.e. the slender spindle and the lamellar capsules.

It is of interest to note that our scaling analysis predicts the existence of a third type of strain-hardening steady-state extensional dynamics for very large membrane hardness C for a given capsule extension L_c (i.e. $C \gg L_c/a$) where the lateral tension normal stress should dominate the restoring membrane forces. (See the second term on the right-hand side of (4.9).) Thus, these capsules resemble more the bubbles which are mainly stabilized via the lateral surface tension forces (Acrivos 1983). We emphasize that this type of strain-hardening extensional dynamics may be more appropriate for non-spherical capsules which can be deformed even for very large membrane hardness.

Both our computational results and our scaling analysis show that Skalak capsules with $C \geqslant 0.5$ have a strong strain-hardening nature that enables them to withstand the highest flow rates in extensional flows. In essence, these capsules will elongate as the flow rate increases and be able always to reach a steady-state shape. For a real strain-hardening capsule, interfacial breaking results from membrane rupture, i.e. material failure, and not from the existence of a critical flow rate. Increasing the membrane

hardness C in these capsules, means that the area-dilatation modulus G_a is increased (for a given shear modulus G_s) and thus the capsule's slender shape becomes more axisymmetric-like in extensional flows to reduce the surface area increase.

For a Skalak capsule with a lower hardness, such as the $C = 0.1$ capsule studied in this paper, its slender shape needs to be flattened at high flow rates, so that the capsule is able to increase its restoring membrane forces due to the area-dilatation resistance, and thus be able to reach steady state. The same is true for the neo-Hookean capsule which in planar extensional flows is the hardest membrane of the strain-softening Mooney–Rivlin family (see e.g. Barthès-Biesel *et al.* 2002; Dodson & Dimitrakopoulos 2009).

Our theoretical investigation has considered moderate to large capsule deformations, while the current, very limited experimental studies at extensional flows involve small to moderate capsule deformations owing to experimental limitations (Barthès-Biesel 1991; Chang & Olbricht 1993*a*). Therefore, we hope that our study motivates for more experiments at high flow rates for both strain-hardening and strain-softening capsules. These experiments can be performed in classical or microfluidic four-roll mill devices (Bentley & Leal 1986; Ha & Leal 2001; Hudson *et al.* 2004).

The steady-state deformation results we provide in § 3 can be used to identify the elastic properties of a real capsule, i.e. the membrane's shear and area-dilatation moduli, by comparing our computation data with experimental measurements of the capsule dimensions at planar extensional flows (Bentley & Leal 1986; Ha & Leal 2001; Hudson *et al.* 2004). This procedure has the advantage of not depending on, or being influenced by, the fluids' viscosity ratio or the membrane viscosity (if any). We emphasize that the proposed determination of both membrane moduli utilizes a single experimental technique, instead of the commonly required two different experiments (Pieper *et al.* 1998; Koleva & Rehage 2012). To achieve this, we utilize both the length L_c and width S_c of the capsule (and not the single deformation parameter $D = (L_c - S_c)/(L_c + S_c)$), and we propose investigation in moderate and high flow rates where the effects of the membrane hardness become prominent and thus capsules with different area-dilatation modulus can be identified. It is of interest to point out that our proposed procedure may also be valid for other flow types.

Our current investigation, which is concentrated on the steady-state capsule dynamics, may provide useful physical insight on the transient capsule dynamics in extensional-type flows owing to the quasi-steady nature of low-Reynolds-number flows. In addition, our theoretical work may provide useful physical insight for the extensional dynamics of other soft particles, including erythrocytes, which are able to withstand strong flow rates and thus show large flow deformations. We emphasize that the pointed profiles of our shapes resemble the elongated and pointed profiles of erythrocytes in strong shear flows occurring owing to the extensional component of this flow type; see for example figure 2 in the work of Fischer, Stöhr-Liesen & Schmid-Schönbein (1978). The erythrocyte membrane consists of an outer lipid bilayer (which is essentially a two-dimensional incompressible fluid with no shearing resistance as in vesicles) and an underlying spectrin skeleton (which exhibits shearing and area-dilatation resistance like the elastic membrane of common artificial capsules) (Skalak, Özkaya & Skalak 1989). Under different flow conditions, the spectrin cytoskeleton dominates the erythrocyte dynamics and the cell behaves like a non-spherical capsule (Skotheim & Secomb 2007; Dodson & Dimitrakopoulos 2010).

Acknowledgements

This work was supported in part by the National Science Foundation. Most computations were performed on multiprocessor computers provided by the Extreme

Science and Engineering Discovery Environment (XSEDE) which is supported by the National Science Foundation.

REFERENCES

ACRIVOS, A. 1983 The breakup of small drops and bubbles in shear flows. *Ann. N.Y. Acad. Sci.* **404**, 1–11.

ALEXEEV, A. & BALAZS, A. C. 2007 Designing smart systems to selectively entrap and burst microcapsules. *Soft Matt.* **3**, 1500–1505.

BARTHÈS-BIESEL, D. 1991 Role of interfacial properties on the motion and deformation of capsules in shear flow. *Physica* A **172**, 103–124.

BARTHÈS-BIESEL, D., DIAZ, A. & DHENIN, E. 2002 Effect of constitutive laws for two-dimensional membranes on flow-induced capsule deformation. *J. Fluid Mech.* **460**, 211–222.

BARTHÈS-BIESEL, D. & RALLISON, J. M. 1981 The time-dependent deformation of a capsule freely suspended in a linear shear flow. *J. Fluid Mech.* **113**, 251–267.

BENTLEY, B. J. & LEAL, L. G. 1986 An experimental investigation of drop deformation and breakup in steady, two-dimensional linear flows. *J. Fluid Mech.* **167**, 241–283.

CARIN, M., BARTHÈS-BIESEL, D., EDWARDS-LÉVY, F., POSTEL, C. & ANDREI, D. C. 2003 Compression of biocompatible liquid-filled HSA-alginate capsules: determination of the membrane mechanical properties. *Biotechnol. Bioengng* **82**, 207–212.

CHABERT, M. & VIOVY, J.-L. 2008 Microfluidic high-throughput encapsulation and hydrodynamic self-sorting of single cells. *Proc. Natl Acad. Sci. USA* **105**, 3191–3196.

CHANG, K. S. & OLBRICHT, W. L. 1993*a* Experimental studies of the deformation of a synthetic capsule in extensional flow. *J. Fluid Mech.* **250**, 587–608.

CHANG, K. S. & OLBRICHT, W. L. 1993*b* Experimental studies of the deformation and breakup of a synthetic capsule in steady and unsteady simple shear flow. *J. Fluid Mech.* **250**, 609–633.

CRANSTON, H. A., BOYLAN, C. W., CARROLL, G. L., SUTERA, S. P., WILLIAMSON, J. R., GLUZMAN, I. Y. & KROGSTAD, D. J. 1984 Plasmodium falciparum maturation abolishes physiologic red cell deformability. *Science* **223**, 400–403.

DIMITRAKOPOULOS, P. 2012 Analysis of the variation in the determination of the shear modulus of the erythrocyte membrane: Effects of the constitutive law and membrane modeling. *Phys. Rev.* E **85**, 041917.

DODSON, W. R. III & DIMITRAKOPOULOS, P. 2008 Spindles, cusps and bifurcation for capsules in Stokes flow. *Phys. Rev. Lett.* **101**, 208102.

DODSON, W. R. III & DIMITRAKOPOULOS, P. 2009 Dynamics of strain-hardening and strain-softening capsules in strong planar extensional flows via an interfacial spectral boundary element algorithm for elastic membranes. *J. Fluid Mech.* **641**, 263–296.

DODSON, W. R. III & DIMITRAKOPOULOS, P. 2010 Tank-treading of erythrocytes in strong shear flows via a non-stiff cytoskeleton-based continuum computational modeling. *Biophys. J.* **99**, 2906–2916.

FIDDES, L. K., YOUNG, E. W. K., KUMACHEVA, E. & WHEELER, A. R. 2007 Flow of microgel capsules through topographically patterned microchannels. *Lab on a Chip* **7**, 863–867.

FISCHER, T. M., STÖHR-LIESEN, M. & SCHMID-SCHÖNBEIN, H. 1978 The red cell as a fluid droplet: tank tread-like motion of the human erythrocyte membrane in shear flow. *Science* **202**, 894–896.

HA, J. W. & LEAL, L. G. 2001 An experimental study of drop deformation and breakup in extensional flow at high capillary number. *Phys. Fluids* **13**, 1568–1576.

HIGLEY, M., SIEGEL, M. & BOOTY, M. R. 2012 Semi-analytical solutions for two-dimensional elastic capsules in Stokes flow. *Proc. R. Soc. Lond.* A **468**, 2915–2938.

HINCH, E. J. & ACRIVOS, A. 1979 Steady long slender droplets in two-dimensional straining motion. *J. Fluid Mech.* **91**, 401–414.

HUDSON, S. D., PHELAN, F. R., HANDLER JR, M. D., CABRAL, J. T., MIGLER, K. B. & AMIS, E. J. 2004 Microfluidic analog of the four-roll mill. *Appl. Phys. Lett.* **85** (2), 335–337.

KOLEVA, I. & REHAGE, H. 2012 A comparison of different experimental methods for investigating the mechanical properties of plane polysiloxane membranes and capsule walls. *Soft Matt.* **8**, 7672–7682.

KESSLER, S., FINKEN, R. & SEIFERT, U. 2008 Swinging and tumbling of elastic capsules in shear flow. *J. Fluid Mech.* **605**, 207–226.

KUMAR, A. & GRAHAM, M. D. 2012 Margination and segregation in confined flows of blood and other multicomponent suspensions. *Soft Matt.* **8**, 10536–10548.

KURIAKOSE, S. & DIMITRAKOPOULOS, P. 2011 Motion of an elastic capsule in a square microfluidic channel. *Phys. Rev.* E **84**, 011906.

KURIAKOSE, S. & DIMITRAKOPOULOS, P. 2013 Deformation of an elastic capsule in a rectangular microfluidic channel. *Soft Matt.* **9**, 4284–4296.

LAC, E., BARTHÈS-BIESEL, D., PELEKASIS, N. A. & TSAMOPOULOS, J. 2004 Spherical capsules in three-dimensional unbounded Stokes flows: effect of the membrane constitutive law and onset of buckling. *J. Fluid Mech.* **516**, 303–334.

LECLERC, E., KINOSHITA, H., FUJII, T. & BARTHÈS-BIESEL, D. 2012 Transient flow of microcapsules through convergent-divergent microchannels. *Microfluid Nanofluid* **12**, 761–770.

LENSEN, D., BREUKELEN, K. V., VRIEZEMA, D. M. & HEST, J. C. M. V. 2010 Preparation of biodegradable liquid core PLLA microcapsules and hollow PLLA microcapsules using microfluidics. *Macromol. Biosci.* **10**, 475–480.

MOHANDAS, N. & CHASIS, J. A. 1993 Red blood cell deformability, membrane material properties and shape: regulation by transmembrane, skeletal and cytosolic proteins and lipids. *Sem. Hem.* **30**, 171–192.

PARK, S.-Y. & DIMITRAKOPOULOS, P. 2013 Transient dynamics of an elastic capsule in a microfluidic constriction. *Soft Matt.* **9**, 8844–8855.

PIEPER, G., REHAGE, H. & BARTHÈS-BIESEL, D. 1998 Deformation of a capsule in a spinning drop apparatus. *J. Colloid Interface Sci.* **202**, 293–300.

POPEL, A. S. & JOHNSON, P. C. 2005 Microcirculation and Hemorheology. *Annu. Rev. Fluid Mech.* **37**, 43–69.

POZRIKIDIS, C. 2001 Interfacial dynamics for Stokes flow. *J. Comput. Phys.* **169**, 250–301.

POZRIKIDIS, C. (Ed.) 2003 *Modeling and Simulation of Capsules and Biological Cells*. Chapman and Hall.

PREVOT, M., CORDEIRO, A. L., SUKHORUKOV, G. B., LVOV, Y., BESSER, R. S. & MÖHWALD, H. 2003 Design of a microfluidic system to investigate the mechanical properties of layer-by-layer fabricated capsules. *Macromol. Mater. Eng.* **288**, 915–919.

RACHIK, M., BARTHÈS-BIESEL, D., CARIN, M. & EDWARDS-LEVY, F. 2006 Identification of the elastic properties of an artificial capsule membrane with the compression test: effect of thickness. *J. Colloid Interface Sci.* **301**, 217–226.

SEIFFERT, S., THIELE, J., ABATE, A. R. & WEITZ, D. A. 2010 Smart microgel capsules from macromolecular precursors. *J. Am. Chem. Soc.* **132**, 6606–6609.

SKALAK, R., TOZEREN, A., ZARDA, R. P. & CHIEN, S. 1973 Strain energy function of red blood cell membranes. *Biophys. J.* **13**, 245–264.

SKALAK, R., ÖZKAYA, N. & SKALAK, T. C. 1989 Biofluid mechanics. *Annu. Rev. Fluid Mech.* **21**, 167–204.

SKOTHEIM, J. M. & SECOMB, T. W. 2007 Red blood cells and other nonspherical capsules in shear flow: oscillatory dynamics and the tank-treading-to-tumbling transition. *Phys. Rev. Lett.* **98**, 078301.

TAYLOR, G. I. 1934 The formation of emulsions in definable fields of flow. *Proc. R. Soc. Lond.* A **146**, 501–523.

WALTER, J., SALSAC, A. V., BARTHÈS-BIESEL, D. & LE TALLEC, P. 2010 Coupling of finite element and boundary integral methods for a capsule in a Stokes flow. *Intl J. Numer. Meth. Engng* **83**, 829–850.